



HAL
open science

Tricritical point and suppression of the Shastry-Sutherland phase in $\text{Ce}_2(\text{Pd}_{1-x}\text{Ni}_x)_2\text{Sn}$

Julián Sereni, Guy Schmerber, Mariano Gómez Berisso, Bernard Chevalier,
Jean-Paul Kappler

► **To cite this version:**

Julián Sereni, Guy Schmerber, Mariano Gómez Berisso, Bernard Chevalier, Jean-Paul Kappler. Tricritical point and suppression of the Shastry-Sutherland phase in $\text{Ce}_2(\text{Pd}_{1-x}\text{Ni}_x)_2\text{Sn}$. *Physical Review B: Condensed Matter and Materials Physics* (1998-2015), 2012, 85 (13), 134404 (6 p.). 10.1103/PhysRevB.85.134404 . hal-00688050

HAL Id: hal-00688050

<https://hal.science/hal-00688050>

Submitted on 30 Aug 2023

HAL is a multi-disciplinary open access archive for the deposit and dissemination of scientific research documents, whether they are published or not. The documents may come from teaching and research institutions in France or abroad, or from public or private research centers.

L'archive ouverte pluridisciplinaire **HAL**, est destinée au dépôt et à la diffusion de documents scientifiques de niveau recherche, publiés ou non, émanant des établissements d'enseignement et de recherche français ou étrangers, des laboratoires publics ou privés.

Tricritical point and suppression of the Shastry-Sutherland phase in $\text{Ce}_2(\text{Pd}_{1-x}\text{Ni}_x)_2\text{Sn}$ J. G. Sereni,^{1,*} G. Schmerber,² M. Gómez Berisso,¹ B. Chevalier,³ and J. P. Kappler²¹*División Bajas Temperaturas, CAB-CNEA and Conicet, 8400 S. C. de Bariloche, Argentina*²*Institut de Physique et Chimie de Strasbourg, UMR 7504 CNRS-UDS, 23 rue du Loess, B.P. 43, F-67034 Strasbourg Cedex 2, France*³*Centre National de la Recherche Scientifique, Université de Bordeaux, ICMCB, 87 av. Dr. Schweitzer, F-33608 Pessac Cedex, France*

(Received 11 October 2011; revised manuscript received 22 February 2012; published 2 April 2012)

Structural, magnetization, and heat capacity measurements were performed on $\text{Ce}_2(\text{Pd}_{1-x}\text{Ni}_x)_2\text{Sn}$ compounds covering the full range of the Mo_2FeB_2 structure stability ($0 \leq x \leq 0.25$). In this system, the two transitions observed in $\text{Ce}_2\text{Pd}_2\text{Sn}$ (antiferromagnetic $T_N = 4.8$ K and ferromagnetic $T_C = 2.1$ K) converge into a tricritical point at $T_{\text{cr}} \approx 3.4$ K for $x_{\text{cr}} \approx 0.3$, where the intermediate antiferromagnetic (AF) phase is suppressed. The decrease of the $T_N(x)$ phase boundary is due to an incipient Kondo screening of the Ce-4*f* moments. This effect and the increase of local atomic disorder affect the formation of Ce-magnetic dimers on which the Shastry-Sutherland lattice (SSL) builds up. On the contrary, the $T_C(x)$ transition to the ferromagnetic ground state increases as a consequence of the weakening of the intermediate phase. Applied magnetic fields also suppress the AF-SSL phase as it was already observed in the stoichiometric compound.

DOI: [10.1103/PhysRevB.85.134404](https://doi.org/10.1103/PhysRevB.85.134404)

PACS number(s): 75.40.-s, 75.30.Hx, 75.30.Mb

I. INTRODUCTION

Crystalline structures with local symmetries which favor magnetic frustration attract special interest because they provide the scenario for novel phase formation. In many cases, magnetic frustration or exotic phases occur in competition with classical long-range order ground states (GS). Thus, the search of exotic phases is addressed to the vicinity of magnetic transitions where the first term of the Landau-Ginsburg free energy expansion $G(\psi)$ tends to zero. The consequent broadening of the $G(\psi)$ minimum favors the access to alternative minima produced by local free energy “roughness” as a function of a nontrivial order parameter.¹ Those minima compete in energy for the formation of novel phases, which may become unstable under small variations of control parameters like magnetic field, alloying, or pressure.

Besides frustrated magnetic configurations, alternative phases may occur under peculiar geometrical conditions. Among them, the so-called Shastry-Sutherland lattice (SSL)^{2,3} builds up from mutually orthogonal magnetic dimers which impose further topological and magnetic constraints. This peculiar lattice can be described as a two-dimensional simple squared lattice, where nearest-neighbor (*nn*) and next-nearest-neighbor coupling are antiferromagnetic. In the case where *nn* magnetic atoms form dimers disposed in an orthogonal network, the configuration is topologically equivalent to the two-dimensional square-lattice Heisenberg model.³

These conditions are realized in some members of the R_2T_2X family of compounds (with $R =$ rare earths or actinides, $T =$ transition metals, and $X = p$ metalloids), which crystallize in tetragonal Mo_2FeB_2 structure.⁴ In that structure, each R layer forms a mosaic of magnetic atoms coordinated as isosceles triangles between nearest and next-nearest neighbors centered on the z axis of the T element. The shortest side of those triangles, where R - R magnetic dimers form, is shared by two consecutive triangles like in the shortest diagonal of a rhombohedron. The resulting simple square lattice of mutually orthogonal rhombohedron mimics a sort of pinwheel centered on the z axis of the X element,⁵ whereas the net of dimers forms a simple two-dimensional (2D) square lattice.

Recently, SSL phases were found in a number of R_2T_2X compounds^{5,6} and the involved magnetic interactions theoretically discussed.⁷ In Ce_2Pd_2X compounds, where Ce-Ce dimers form through a nearest-neighbor ferromagnetic (FM) interaction, the SSL phase shows up within a limited range of temperature (between $T_N = 4.8$ K and $T_C = 2.1$ K in $\text{Ce}_2\text{Pd}_2\text{Sn}$ ⁸). Below T_C , an FM-GS takes over undergoing a first-order transition due to the discontinuity in the order parameter. Further studies performed under magnetic field on the mentioned compound⁹ showed that the intermediate phase is suppressed by a magnetic field $B_{\text{cr}} \approx 0.12$ T at $T_{\text{cr}} \approx 3.2$ K. The fact that the SSL phase is suppressed by quite low magnetic field in $\text{Ce}_2\text{Pd}_2\text{Sn}$ highlights its instability with respect to a three-dimensional (3D) FM magnetic GS structure.

In this work we have investigated Ni-doped $\text{Ce}_2(\text{Pd}_{1-x}\text{Ni}_x)_2\text{Sn}$ alloys with the scope to compare the effect of chemical pressure and magnetic field on the stability of the SSL phase. The effective pressure is induced by the Ce-ligands substitution since Ni and Pd are isoelectronic elements with Ni atoms about 25% smaller in volume than Pd ones. Thus, this effective pressure is expected to weaken the 4*f*-Ce magnetic moments. Coincidentally, applied magnetic field shall progressively suppress the SSL phase in those alloys like in the stoichiometric compound. In a recent study, a change of structure was detected at $x = (0.35 \pm 0.05)$.¹⁰ Since beyond a short range of coexistence of two phases, this system stabilizes in an orthorhombic W_2CoB_2 -type structure for $x > 0.4$, the large ρ_0 values and the abnormal $\rho(T)$ dependence can be explained by the presence of nonsingle phases in the concentration region where the system presents a coexistence of two crystalline structures. As expected there is a reduction of the unit cell volume of the Ni-rich phase with respect to the Pd-rich one.

II. EXPERIMENTAL DETAILS AND RESULTS

The details of the sample preparation were described in a previous paper.⁵ Structural characterization confirms the single-phase composition of the samples in a tetragonal

Mo₂FeB₂-type structure for $x < 0.3$. The actual composition of the stoichiometric compound was determined to be Ce_{2.005}Pd_{1.988}Sn_{0.997} after SEM/EDAX analysis. Lattice parameters slightly decrease with Ni concentration from $a = 7.765$ Å and $c = 3.902$ Å for $x = 0$, to $a = 7.7122$ Å and $c = 3.8941$ Å for $x = 0.25$. These variations drive a reduction of the unit cell volume of about $\approx 1.5\%$ between $x = 0$ and 0.25 . On the contrary, the c/a ratio does not change significantly, indicating that nearest-neighbor distances change proportionally in both directions.

DC-magnetization measurements were carried out using a Quantum Design MPMS magnetometer operating between 2 and 300 K, and magnetic fields up to 5 T. Specific heat was measured using the standard heat pulse technique in a semiadiabatic He³ calorimeter within the 0.5- to 20-K range of temperature, at zero and under applied magnetic field up to 4 T. The $4f$ electron contribution to the specific heat (C_m) was obtained by subtracting the phonon contribution extracted from the isotopic La₂Pd₂Sn compound. Electrical resistivity was measured between 0.5 K and room temperature using a standard four-probe technique with a LR700 bridge. However, sample cracking impedes to extract valuable information from the $\rho(T)$ data.

A. Ni-concentration-dependent properties

As shown in Fig. 1, Ni doping does not affect significantly the magnetic susceptibility (χ , defined by the M/B ratio) at high temperature. The fits of $\chi(T) = \sum_0^2 \mu_i^2 * \exp(-\Delta_i/T)/(T - T_I) * Z$ do not lead to significant variations of crystal field effect (CEF) parameters with respect to the values observed in stoichiometric Ce₂Pd₂Sn,⁵ namely, $\Delta_I = (65 \pm 5)$ K and $\Delta_{II} = (240 \pm 10)$ K. From the inverse of $\chi(T)$, one extracts that the high temperature ($T \leq 70$ K) θ_p^{HT} slightly changes only for $x \geq 0.2$ from -16 K to -25 K. This indicates a small hybridization increase coming from the CEF excited levels within that range of Ni concentration. Coincidentally, the high-temperature Ce magnetic moment does not deviate significantly from its Ce³⁺ theoretical value.

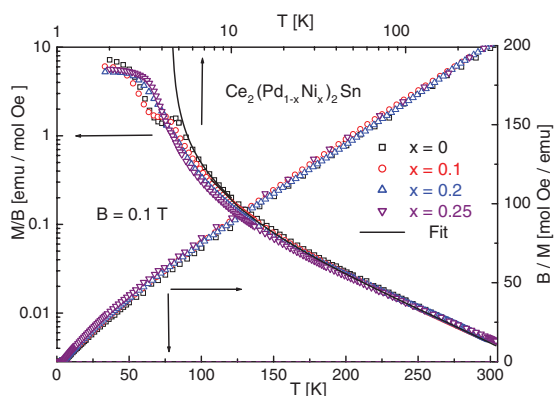


FIG. 1. (Color online) High-temperature magnetic susceptibility, defined as M/B , in a log-log representation for different Ni concentrations (left and upper axes) and inverse B/M (right and lower axes). The continuous line corresponds to the fit described in the text, applied on sample $x = 0$ results.

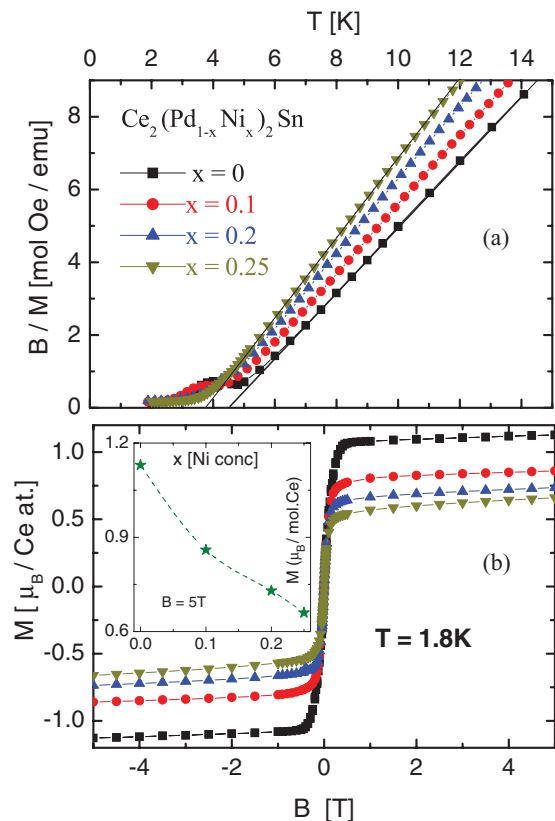


FIG. 2. (Color online) (a) Low-temperature inverse B/M values showing the $\theta_p^{\text{LT}}(x)$ variation, measured with $B = 0.1$ T. (b) Field magnetization in the FM phase of $x = 0$ sample, showing the decrease of the saturation moment with Ni increase. (Inset) Magnetic moment at $B = 5$ T within the $x \leq 0.25$ range.

However, at low temperature, $\theta_p^{\text{LT}}(T \rightarrow 0)$ values decrease from 4.5 K ($x = 0$) to 3.7 K ($x = 0.25$) [see Fig. 2(a)], indicating a moderate Ni doping effect on the GS doublet. This goes hand in hand with the magnetic saturation extracted from field-dependent magnetization measurements performed at $T = 1.8$ K within the FM phase, shown in Fig. 2(b). Moreover, the cusp of $M(T)$ at $T = T_N$ shifts to lower temperature (from 4.8 K for $x = 0$ to 3.9 K for $x = 0.2$). Then, at $x = 0.25$, the AF phase is overcome by the FM contribution [see Fig. 4(a)].

Figure 3 shows the variation of $C_m(T)$ jumps as a function of Ni concentration. While the temperature of the upper one decreases from $T_N(x = 0) = 4.8$ K to $T_N(x = 0.25) \approx 3.5$ K, the lower transition increases from $T_C(x = 0) = 2.1$ K up to $T_C(x = 0.25) \approx 3.3$ K. The respective concentration dependencies are represented in the inset of Fig. 4(a). These opposite Ni dependencies drive the transitions to merge in a tricritical point at $T_{\text{cr}} \approx 3.4$ K, just above the highest Ni concentration studied ($x = 0.25$).

The transition at $T_N(x)$ is of second order, whereas that at $T_C(x)$ is of first order.⁵ This character is recognized by an hysteretic $C_m(T)$ dependence measured around T_C and reflects the discontinuity in the magnetic order parameter at $T = T_C$. Both $C_m(T)$ maxima decrease with Ni doping, however, as they merge into a unique maximum the $C_m(T)$ cusp rises. Notice that the cusp of the $x = 0.25$ sample is sharper than that of the $T_N(x = 0.2)$ but similar to that of $T_C(x = 0.2)$, indicating

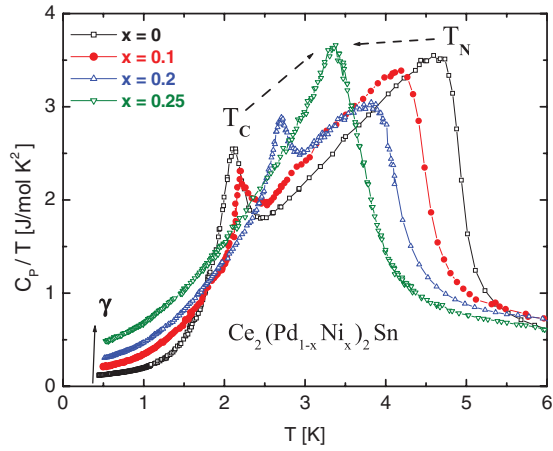


FIG. 3. (Color online) Thermal dependence of C_m/T for different Ni concentrations, showing how AF- T_N and FM- T_C transitions merge at $x_{cr} \geq 0.25$. Arrow identified with γ represents a rising heavy fermion component contribution.

that both transitions merge at that concentration lying at the proximity to the critical point.

B. Magnetic field effects

The Ni doping and magnetic field effects both enhance the FM character of the GS phase with the consequent $T_C(x, B)$ increase. On the contrary, while Ni doping produces a decrease

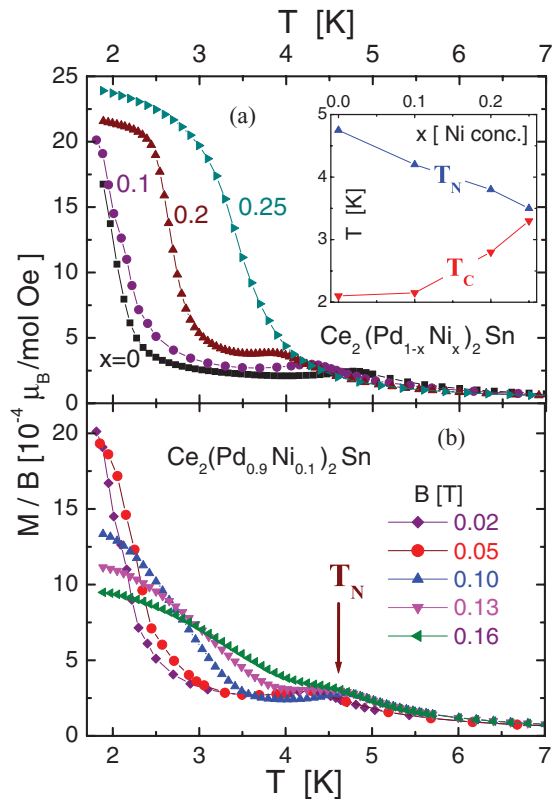


FIG. 4. (Color online) Comparison of the thermal dependence of magnetization around AF and FM transitions (a) as a function of Ni doping (with $B = 0.02$ T). (Inset) $T_N(x)$ and $T_C(x)$ dependencies. (b) Magnetic field effect on the $x = 0.1$ sample.

of $T_N(x)$ magnetic field does not significantly affect the upper transition. The doping effect can be observed in Fig. 4(a), which shows how the temperature of the spontaneous magnetization (related to T_C) increases, overlapping the $M(T_N)$ cusp as Ni content increases.

As shown in Fig. 4(b) for $x = 0.1$, whatever the applied magnetic field, the temperature of the $M(T_N)$ cusp remains almost unchanged. The same behavior was observed in the stoichiometric compound⁹ and for $x = 0.2$. In the case of the sample with $x = 0.25$, the T_N cusp is overlapped by the FM signal already at very low applied field. Here one has to take into account that, apart from the $T_C(x)$ increase, the FM transition is intrinsically smeared under applied magnetic field. Hence, the high temperature tail of the FM magnetization overcomes the T_N cusp faster than the actual increase of $T_C(x)$.

III. DISCUSSION

A. Specific heat gap

Relevant information related to the magnetic structure of this system can be extracted from the analysis of the thermal dependence of the specific heat within the ordered phase. Since the $x = 0$ sample has shown strong anisotropy in the magnon spectrum, we have analyzed the magnetic contribution of the FM phase to $C_m(T)$ by fitting all curves with a unique function in order to evaluate the variation of the characteristic parameters as a function of Ni content. The simplest applicable function is $C_m/T = \gamma + AT^2 \exp(-E_g/T)$,¹¹ where the γ term accounts for the electronic degrees of freedom behaving as Kondo liquid, the coefficient A is inversely proportional to the strength of the magnetic interaction,¹² and E_g represents the energy (expressed in temperature) of the gap of anisotropy in the magnon spectrum. Respective fits are included in Fig. 5 in addition to the computed values of $\gamma(x)$ and $E_g(x)$ in the inset. These results indicate that the specific heat behaves as the systems whose gap of anisotropy decreases when approaching the critical concentration due to the reduction of its anisotropic character. Coincidentally, the γ contribution increases with Ni content.

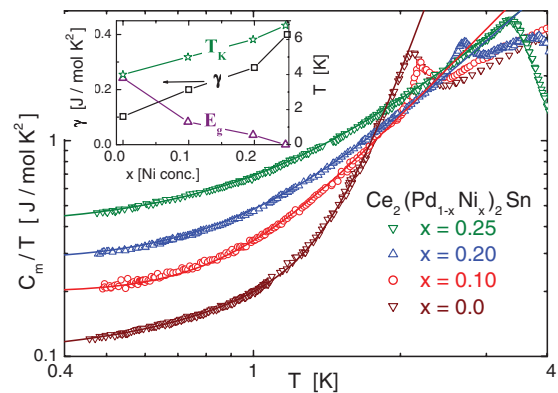


FIG. 5. (Color online) Analysis of the $C_m(T)/T$ dependence for $T < T_C$ in a log-log representation. γ and magnon gaps E_g are extracted from the fit (continuous lines); see the text. (Inset) Ni concentration dependence of $\gamma(x)$ (left axis), and $E_g(x)$ and Kondo temperature $T_K(x)$ (right axis).

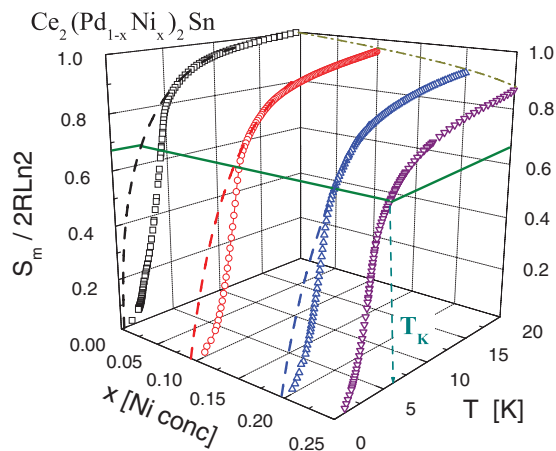


FIG. 6. (Color online) Thermal dependence of the entropy for the studied samples in a 3D representation. Dashed curves indicate the extrapolation of $S_m(T)$ from $T > T_N$ to $T < T_N$, and the straight lines the $S_m = 0.66 \times 2R \ln 2$ value from which T_K is extracted.

B. Entropy and Kondo temperature

The thermal variation of the magnetic contribution to the entropy (S_m) as a function of Ni doping is presented in Fig. 6. There one can see that some incipient hybridization effects can be detected only for $x \geq 0.2$. In order to extract the Kondo temperature variation, we apply the current Desgranges-Schotte criterium¹³ from which at $T = T_K$ the entropy reaches the value $S_m = 0.66 R \ln 2$. Notice that in our case the comparison has to be done in $2R \ln 2$ units because there are two Ce atoms contained in a formula unit of this compound. As this model was proposed for single impurities, the $S_m(T)$ curve has to be extrapolated from $T > T_N$ following the curvature within the noninteracting (paramagnetic) phase, which does not account for the condensation of degrees of freedom into the ordered state. Despite the small error introduced by this extrapolation, the relevant information is the low value of T_K ($T_K \approx 4$ K for $x = 0$) and its variation with concentration ($T_K \approx 7$ K for $x = 0.25$). The computed T_K values are included in the inset of Fig. 5. There is an apparent contradiction in this coincident increase of T_K and γ with x because they are expected to depend inversely on each other (i.e., $\gamma \propto 1/T_K$ ¹³). This behavior can be explained by the fact that T_K is an *intensive* parameter (i.e., a scale of energy) which increases with x , and γ is *pseudointensive* because it depends on the degrees of freedom involved in the Kondo liquid contribution. From this comparison we conclude that there is a gradual transference of degrees of freedom from the ordered phase (with local $4f$ character) to the Kondo liquid component (of itinerant character) that dominates the $\gamma(x)$ variation.

C. Stability of the SSL phase versus doping

In order to investigate up to which extent Ni doping affects the stability of the SSL phase, we have studied the magnetic field effect in the alloyed samples following the same procedure applied to the stoichiometric compound ($x = 0$).⁹ Starting with the $x = 0.1$ sample [see Fig. 7(a)], we have performed $M(B)$ measurements within the range of temperature where the features related to the SSL phase

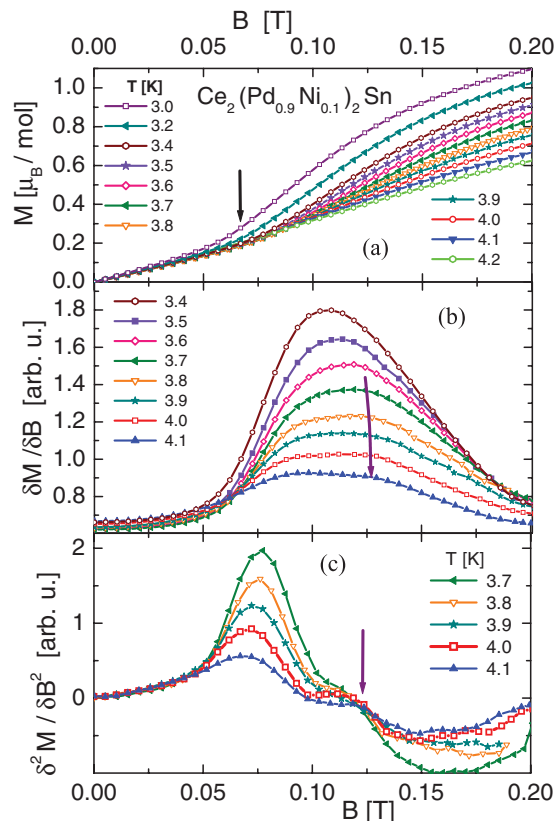


FIG. 7. (Color online) (a) Field dependence of magnetization in sample $x = 0.1$ between 3 and 4.2 K. The arrow indicates the onset of the field-induced polarization. (b) First derivative with an arrow indicating an incipient shoulder; see the text. (c) Second derivative for the $3.7 \text{ K} \leq T \leq 4.1 \text{ K}$ range, with the arrow indicating the satellite anomaly.

may be detected. Above T_C , the $M(B)$ isotherms show an S shape reflecting an AF character which is rapidly polarized by magnetic field [see the arrow in Fig. 7(a)]. There is, however, a crossing of magnetization curves around $B = 0.11$ T followed by a slight modulation which was taken as indication of an SSL formation in the stoichiometric compound.⁹ More detailed information was extracted from the $\partial M / \partial B|_T$ derivative [see Fig. 7(b)] where an incipient shoulder can be appreciated at $B \approx 0.12$ T for the $3.7 \text{ K} \leq T \leq 4.1 \text{ K}$ temperature range [see the arrow in Fig. 7(b)]. As this feature was taken as an indication of the incipient $M(B)$ step related to the SSL phase, we have analyzed also the second $\partial^2 M / \partial B^2|_T$ derivative of the $M(B)$ results. The curves for different temperatures [see Fig. 7(c)] allows one to determine the onset of the induced FM phase (main maximum at $B \approx 0.077$ T) and the satellite anomaly (see the arrow at $B \approx 0.12$ T).

In comparison to the stoichiometric compound, the main maximum decreases from $B \approx 0.11$ to 0.08 T, and the satellite shifts down from $B \approx 0.15$ to 0.12 T with a significant reduction of intensity. Although the B values follow the predictions for an SSL for the appearance of a plateau in the magnetization (at $1/4$ and $1/8$ of the saturated moment³), these results for sample $x = 0.1$ are in the limit of our experimental detection. Indeed, in the following investigated concentration ($x = 0.2$) no traces of the mentioned anomaly were observed

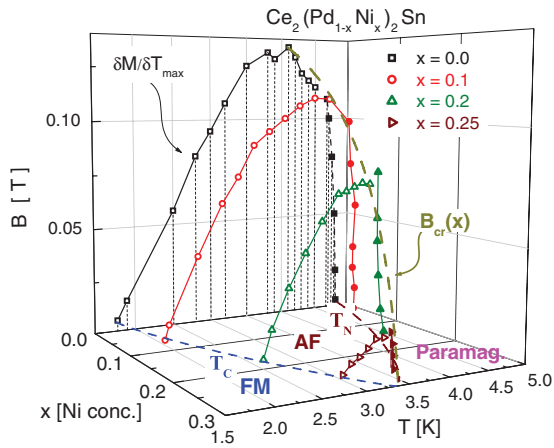


FIG. 8. (Color online) Ni concentration and magnetic-field-dependent phase diagram in a 3D representation. Open symbols correspond to the maximum of $M(T)$ derivative, related to the FM transition observed from specific heat at $B = 0$. Solid symbols correspond to the AF transition at the same concentration. $B_{cr}(x)$ is defined by the maximum field reached by the AF phase.

indicating a border line for the SSL formation at $x \simeq 0.1$. Not only the weakening of Ce magnetic moments but also the local disorder due to the difference between Pd and Ni sizes avoid the Ce-Ce dimer formation with the consequent smearing of the SSL phase.

D. Magnetic phase diagram

The comparison between Ni doping and magnetic field effects is presented in a 3D phase diagram in Fig. 8. The field driven transition between intermediate AF and FM-GS phases is drawn as a function of the temperature of the maximum slope of $M(T)$ (i.e., $\partial M / \partial T|_{\max}$). This is in agreement with the $C_m(T)$ results. Both phase boundaries join at a critical point, which decreases with Ni content from $T_{cr}(x = 0) = (4.2 \pm 0.3)$ K and $B_{cr} = (0.16 \pm 0.02)$ T down to $T_{cr}(x = 0.25) \approx (3.5 \pm 0.3)$ K and $B_{cr} \approx (0.02 \pm 0.005)$ T, placed at the edge of the intermediate phase disappearance (i.e., where $B_{cr} \rightarrow 0$). Unfortunately, the tricritical point, where AF, FM, and paramagnetic phases join together, cannot be reached by doping because it lies beyond the stability limit of the Mo_2FeB_2 crystal structure.

The evolution of AF and FM phase boundaries respond to different effects. Starting from high temperature, the decrease of the upper (AF) transition $T_N(x)$ is expected to come from two mechanisms: (i) the competition between the Kondo effect and RKKY magnetic interactions acting on the Ce-4*f* magnetic moment intensity according to the Doniach-Lavagna model,¹⁴ and (ii) the local atomic disorder introduced by alloying atoms of different sizes. Both effects weaken the

formation of magnetic Ce dimers on which the SSL builds up. On the contrary the $T_C(x)$ increase is a consequence of the intermediate AF phase weakening, like in $\text{Ce}_2\text{Pd}_2\text{Sn}$ under the applied magnetic field.⁹

The effect of magnetic field is qualitatively similar for each concentration accounting that the range of stability of the AF phase is progressively reduced. Notably, the $\partial M / \partial B|_T$ derivative in sample with $x = 0.25$ still displays a weak maximum in a restricted range of field and temperature. This suggests that the critical Ni concentration is not yet reached despite that respective cusps of $C_m(T)$ at $T_N(x)$ and $T_C(x)$ in that sample seem to have converged. Interestingly, the critical temperature T_{cr} reached by doping (at zero field) or by application of magnetic field on the stoichiometric compound is very similar. This confirms the equivalent effect of both Ni doping and magnetic field on the suppression of the intermediate phase.

IV. CONCLUSIONS

We have shown that Ni substitution of Pd in $\text{Ce}_2\text{Pd}_2\text{Sn}$ strongly affects the intermediate AF phase which characterizes this compound. While the $T_N(x)$ transition decreases, $T_C(x)$ increases following a first-order transition line with an end critical point. At zero field, $T_N(x)$ and $T_C(x)$ converge right above the highest Ni concentration studied ($x = 0.25$). The increase of the FM-GS phase is simply due to the fact that the quasi 2D-AF character weakens with respect to the 3D-FM one when the interplane interaction becomes relevant. The progressive weakening of the magnon gap and its disappearance coincides with this behavior.

The SSL phenomenology was hardly recognized from the $M(B)$ dependence except in the 10% doped Ni sample; for higher concentrations (i.e., $x = 0.2$) none of those symptoms have been recognized. Since hybridization effects are only marginal, one concludes that atomic disorder plays an important role inhibiting the SSL phase formation. External magnetic field further weakens the intermediate phase like in the stoichiometric compound, allowing one to define the tricritical point extrapolated at $T_{cr} \approx 3.4$ K and $x = 0.3$, where also $B_{cr} \rightarrow 0$. Unfortunately $x = 0.3$ lies within the structural instability range. Nevertheless, further attempts to get closer to that critical point, and a study the Ni-rich side of the phase diagram are in progress.

ACKNOWLEDGMENTS

The author acknowledges L. Amigo and J. Luzuriaga for magnetic measurements. This work was partially supported by projects PICT 2007-0812 and Universidad de Cuyo 06/C326.

*jsereni@cab.cnea.gov.ar

¹T. R. Kirkpatrick and D. Belitz, *Phys. Rev. B* **67**, 024419 (2003).

²B. S. Shastry and B. Sutherland, *Physica B* **108**, 1069 (1981).

³S. Miyahara and K. Ueda, *Phys. Rev. Lett.* **82**, 3701 (1999).

⁴F. Mirambet, P. Gravereau, B. Chevalier, L. Trut and J. Etourneau, *J. Alloys Compd.* **191**, L1 (1993); M. N. Peron, Y. Kergadallan, J. Rebizant, D. Meyer, S. Zwirner, L. Havela, H. Nakotte, J. C.

- Sprilet, G. M. Kalvius, E. Colineau, J. L. Oddou, C. Jeandey, and J. P. Sanchez, *ibid.* **201**, 203 (1993).
- ⁵J. G. Sereni, M. Gomez-Berisso, A. Braghta, G. Schmerber, and J. P. Kappler, *Phys. Rev. B* **80**, 024428 (2009).
- ⁶M. S. Kim and M. C. Aronson, *J. Phys.: Condens. Matter* **23**, 164204 (2011).
- ⁷B. H. Bernhard, B. Coqblin, and C. Lacroix, *Phys. Rev. B* **83**, 214427 (2011).
- ⁸D. Laffargue, F. Fourgeot, F. Bourée, B. Chevalier, T. Roisnel, and J. Etourneau, *Solid State Commun.* **100**, 575 (1996).
- ⁹J. G. Sereni, M. GomezBerisso, G. Schmerber, and J. P. Kappler, *Phys. Rev. B* **81**, 184429 (2010).
- ¹⁰J. G. Sereni, G. Schmerber, A. Braghta, B. Chevalier, and J. P. Kappler, e-print [arXiv:1103.0190](https://arxiv.org/abs/1103.0190).
- ¹¹L. J. Sundström, in *Handbook for Physics and Chemistry of Rare Earths*, edited by K. A. Gschneidner Jr. and L. Eyring, Vol. I (North Holland, Amsterdam, 1978), Chap. 5.
- ¹²See, for example, E. S. R. Gopal, *Specific Heats at Low Temperatures* (Heywood Books, London, 1966).
- ¹³H.-U. Desgranges and K. D. Schotte, *Phys. Lett. A* **91**, 240 (1982).
- ¹⁴S. Doniach, *Physica B&C* **91**, 231 (1977); C. Lacroix, M. Lavagna, and M. Cyrot, *J. Phys. F* **12**, 745 (1982).